

Ka-Band Systems and Processing Approaches for Simultaneous High-Resolution Wide-Swath SAR Imaging and Ground Moving Target Indication

Advanced RF Sensors and Remote Sensing Instruments 2014
Ka-band Earth Observation Radar Mission 2014

4-7 November 2014

ESA-ESTEC, Noordwijk, The Netherlands

S. V. Baumgartner⁽¹⁾, P. Laskowski⁽¹⁾, M. Younis⁽¹⁾, C. Schaefer⁽²⁾, R. Klein⁽²⁾, D. Petrolati⁽³⁾

⁽¹⁾*Microwaves and Radar Institute, German Aerospace Center (DLR)
Münchener Straße 20, 82234 Oberpfaffenhofen, Germany
Email: stefan.baumgartner@dlr.de*

⁽²⁾*Airbus Defence & Space
88039 Friedrichshafen, Germany*

⁽³⁾*European Space Agency, ESTEC
Keplerlaan 1, 2200 AG Noordwijk ZH, The Netherlands*

INTRODUCTION

Although high-resolution wide-swath (HRWS) SAR imaging and ground moving target indication (GMTI) systems from the system architecture point of view look quite similar (both system types employ multiple receiving (RX) channels arranged along azimuth direction), they generally need to be operated in different modes, in particular with significantly different PRFs. HRWS systems require a comparatively low PRF, reflecting the overall length of the full antenna. The low PRF enables wide-swath imaging, and the multiple RX channels are used for signal spectrum reconstruction. The PRF is ideally chosen such that the uniform sampling condition of the RX antenna array is fulfilled:

$$PRF_{HRWS} = \frac{2v_p}{M \cdot L_{a,RX}} \quad (1)$$

where v_p is the platform velocity, M is the number of RX antennas and $L_{a,RX}$ is the length of a single RX antenna which conventionally also defines the minimum along-track baseline. In contrast, GMTI systems require a high PRF, reflecting the short length of the individual RX antenna. For obtaining good clutter suppression and moving target parameter estimation capabilities, it is desired that the displaced phase center antenna (DPCA) condition between adjacent RX channels is fulfilled. Thus, for a system with given along-track baselines $L_{a,RX}$ the PRF has to be adjusted according to

$$PRF_{DPCA} = \frac{2v_p}{L_{a,RX}} = M \cdot PRF_{HRWS}. \quad (2)$$

By having a closer look at this equation it becomes clear, that in principle classical multi-channel GMTI can be achieved with a HRWS system by simply increasing the PRF by a factor of M . Unfortunately, the high PRF system operation mode prevents both wide-swath GMTI as well as wide-swath SAR imaging. Thus, depending on the PRF, either narrow-swath GMTI or HRWS SAR imaging can be performed, but not both at the same time.

The basic resolution of this conflict we have already addressed in [1][5][6], where we have shown that a simultaneous HRWS SAR imaging and low PRF wide-swath GMTI operation mode is feasible. In the present paper we lay the focus on the HRWS-GMTI processing approaches and on the performance assessment of exemplary HRWS-GMTI system concepts. The work presented in [1] and in the following sections we have carried out in the frame of a contract extension of the ESA-funded TRP Activity "Study of Multi-Channel Ka-Band SARs for Moving Target Indication" [2].

MATHEMATICAL RELATIONSHIPS

For reconstructing a highly ambiguous moving target signal sampled by low PRF the beamformers and reconstruction filters conventionally used for HRWS SAR imaging (see e.g. [4][7][8]) have to be adapted according to the target motion parameters, in particular to the target's line-of-sight velocity and Doppler shift, respectively. A detailed mathematical derivation we have given in [1], where we have adapted the conventional *Maximum Signal Method* from

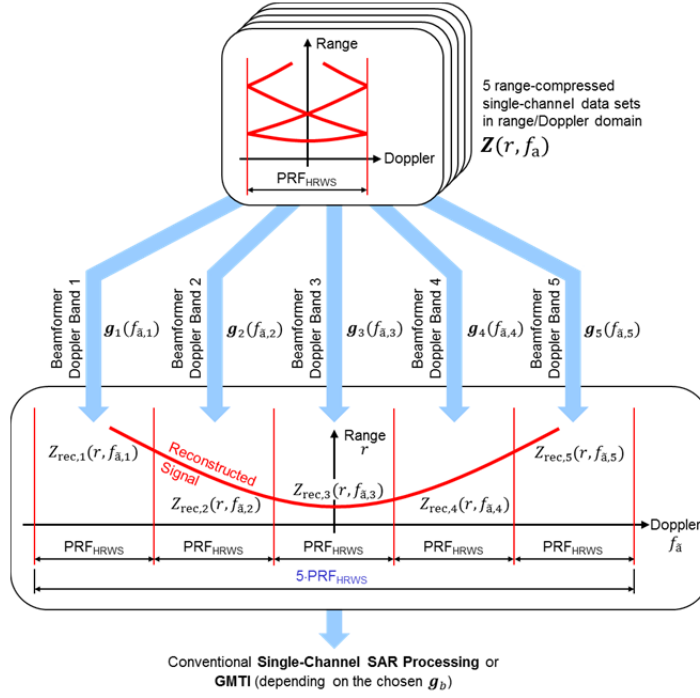


Fig. 1. Basic principle of HRWS reconstruction for an exemplary 5-channel system.

[7][8] so that it also can be used for moving and not only for stationary targets. We have shown that the reconstructed moving target signal can be written as

$$Z_{\text{rec},b}(r, f_{\bar{a},b}) = \mathbf{g}_b^H(u_t, v_{r0}) \cdot \mathbf{Z}(r, f_a) \quad (3)$$

where $\mathbf{g}_b^H(u_t, v_{r0})$ is the beamforming vector adapted to the target's line-of-sight velocity v_{r0} and the directional cosine u_t , \mathbf{Z} is the ambiguous multi-channel signal vector, f_a is the ambiguous Doppler frequency in the range $(-PRF/2 \leq f_a < PRF/2)$, and $f_{\bar{a},b}$ is the unambiguous Doppler frequency for Doppler band b . The adapted beamforming vector is given as

$$\mathbf{g}_b(u_t, v_{r0}) = \frac{1}{G_b(u_t, v_{r0})} \cdot \mathbf{A}(u_t, v_{r0}, \boldsymbol{\vartheta}) \cdot \boldsymbol{\Phi}(u_t, v_{r0}) \cdot \mathbf{1}_M \quad (4)$$

where \mathbf{A} is the antenna pattern matrix, $\mathbf{1}_M$ is a matrix with ones, $\boldsymbol{\vartheta}$ is a parameter vector containing further parameters like range and incidence angle, G_b is a normalization factor taking into account the antenna patterns, and $\boldsymbol{\Phi}$ is the baseline delay matrix.

The basic principle of the signal reconstruction for a 5-channel system is shown in Fig. 1. Depending on the chosen beamformers \mathbf{g}_b either conventional HRWS reconstruction for stationary targets or adapted reconstruction for moving targets can be performed. For reconstructing and focusing a moving target signal the beamformer has to be adapted to the correct line-of-sight velocity of the target. The reconstruction and ambiguity suppression will not be optimal if there is a velocity mismatch. However, just this behavior can be exploited for estimating the velocity with high accuracy by the application of a *Matched Reconstruction Filter Bank* (MRFB) [1]. This even works with a conventional HRWS SAR system without any system modifications. A potential application is high-resolution wide-swath ship monitoring, where not necessarily a clutter suppression capability is required.

HRWS-DPCA ALGORITHM

Especially for targets with low radar cross section (RCS) embedded in a rather strong clutter environment, clutter suppression capability is mandatory. One applicable method is the DPCA technique. For enabling this, M additional RX channels have to be added to a M -channel HRWS SAR system as sketched in Fig. 2 left. The PRF needs not to be increased in this case, i.e., the uniform sampling PRF_{HRWS} can be used. After reconstruction the DPCA condition for the reconstructed FORE and AFT channels is fulfilled.

DPCA clutter suppression is then performed by simply subtracting the coregistered AFT (blue color) from the FORE (red color) channel (cf. Fig. 2 right). Since the target's motion parameters are not known *a priori*, the reconstruction has

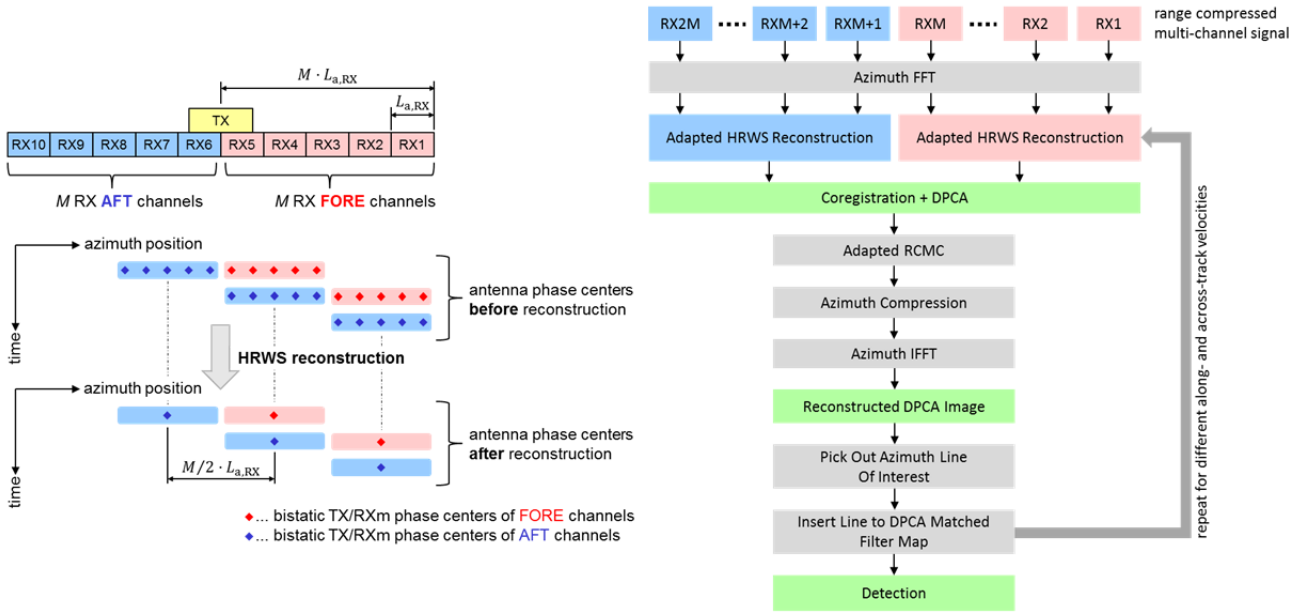


Fig. 2. Principle of the HRWS-DPCA algorithm (left: HRWS system operated with PRF_{HRWS} with M additional RX channels and corresponding bistic phase centers before and after reconstruction ($M=5$ in shown example); right: simplified block diagram with the main processing steps).

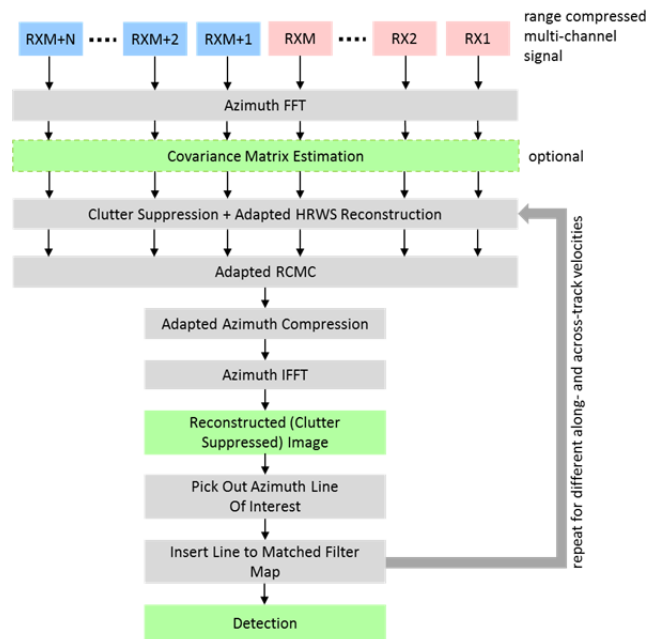


Fig. 3. Principle of the HRWS-STAP algorithm.

to be carried out in a loop where for each iteration different velocity assumptions have to be made (cf. MRFB explained in detail in [1]).

For achieving the same phase center separations as depicted in Fig. 2 left, instead of M additional RX channels principally a subpulse technique can be used as discussed in [1].

HRWS-STAP ALGORITHM

A different approach for clutter suppression is to use Post-Doppler STAP instead of DPCA as depicted in Fig. 3. Here an arbitrary number N of additional RX channels can be added to a M -channel HRWS SAR system. The shown *Covariance Matrix Estimation* block is optional since in principle also a theoretically derived clutter-plus-noise covariance matrix can be used, if the two-way antenna patterns are accurately known.

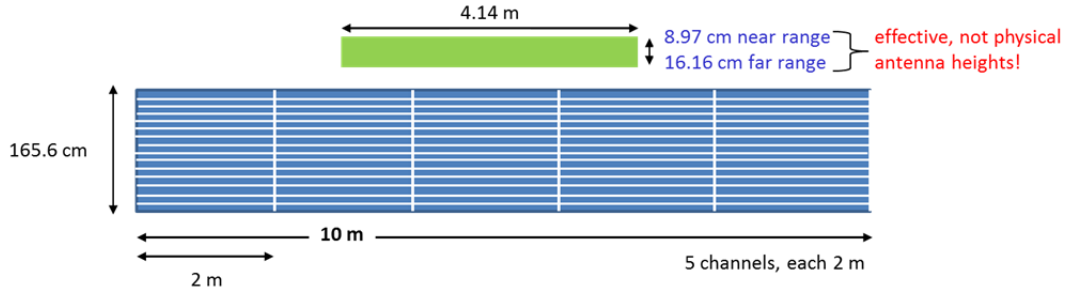


Fig. 4. HRWS reference system with 5 RX channels.

Clutter suppression and motion adapted HRWS reconstruction is carried out in a single step. Instead of the reconstruction described in (3), which is used for the MRFB and the HRWS-DPCA algorithm, for HRWS-STAP the reconstructed signal is obtained by

$$Z_{rec,b}(r, f_{a,b}) = \frac{\mathbf{R}_W^{-1}(f_a) \cdot \mathbf{g}_b(u_t, v_{r0})}{\sqrt{\mathbf{g}_b^H(u_t, v_{r0}) \cdot \mathbf{R}_W^{-1}(f_a) \cdot \mathbf{g}_b(u_t, v_{r0})}} \cdot \mathbf{Z}(r, f_a) \quad (5)$$

where \mathbf{R}_W is the clutter-plus-noise covariance matrix. Meanwhile a conference paper appeared where a similar technique as we suggest is proposed for clutter suppression [9].

HRWS REFERENCE SYSTEM FOR SAR IMAGING

For assessing the performance of a novel HRWS-GMTI system as a first step a conventional 5-channel HRWS SAR system based on reflectarrays was designed for Ka-band. This system is considered as *HRWS Reference System* in the following. For fulfilling the requirements given in Table 1 it is necessary to decrease the orbit height to 400 km if a reasonable overall antenna size shall not be exceeded. Furthermore, the SCan-On-Receive (SCORE) technique is required for each RX channel. For shallower incidence angles or larger slant ranges, it is necessary to switch to a narrower elevation TX beam for increasing the antenna gain. This behavior can principally be implemented using a single reconfigurable reflectarray TX antenna or two different TX antennas.

Table 1. Requirements for the HRWS reference system.

Requirement	Value	Comment
Noise equivalent sigma zero (NESZ)	≤ -18 dB	assumed 4 dB two-way atmospheric attenuation included
Range ambiguity-to-signal ratio (RASR)	≤ -20 dB	
Azimuth ambiguity-to-signal ratio (AASR)	≤ -20 dB	
Azimuth resolution	≤ 1.5 m	
Ground range resolution	≤ 1.5 m	
Ground swath width	≈ 50 km	

The 5-channel HRWS reference system is sketched in Fig. 4 and the corresponding key parameters are listed in Table 2.

HRWS-GMTI SYSTEM CONCEPT AND PERFORMANCE FOR HRWS-DPCA PROCESSING

For the HRWS-DPCA system concept 5 additional RX channels have been added to the HRWS reference system, so that the overall RX antenna length increases to 20 m. In total 10 RX channels are available.

For obtaining the GMTI performance Monte Carlo simulations have been carried out using the novel HRWS-DPCA algorithm. In Fig. 5 the obtained GMTI performance is depicted for three different target RCSs of 10, 3 and -6 dBm². All plots are for an incidence angle of $\theta_i = 34^\circ$ and a clutter reflectivity of -6 dB. The PRF was set to 1533 Hz. The probability of detection is plotted for a desired false alarm rate of 10^{-6} (cf. Fig. 5 top right).

An excellent GMTI performance is achieved for the targets with a RCS of 10 dBm² (blue color) and 3 dBm² (red). The minimum detectable line-of-sight velocity is in the order of 0.5 m/s (cf. Fig. 5 top right) for a false alarm rate of $P_{fa} = 10^{-6}$. The azimuth re-positioning error for the 10 and 3 dBm² targets is better than 30 m outside the blind velocity regions (cf. Fig. 5 bottom left). Even for the target with the comparatively low RCS of -6 dBm² (green color) a

Table 2. Key parameters of the HRWS reference system.

Parameter	Value	Comment
Range bandwidth B_r	270 MHz	ensures a ground range resolution ≤ 1.5 m for incidence angles $\theta_i \geq 22^\circ$
Peak transmit power P_t	3137 W	the available peak power is connected to the range bandwidth
TX losses and atmospheric attenuation L	$1.3 + 4 = 5.3$ dB	4 dB two-way atmospheric attenuation is considered
System noise figure F	4.6 dB	
Duty cycle d_c	0.13	
Center frequency f_c	35.75 GHz	
Orbit height h	400 km	
Platform velocity v_p	7670 m/s	
PRF for uniform sampling PRF_{HRWS}	1533 Hz	
Number of RX channels M	5	
Effective TX antenna height h_{TX} for steep incidence angle	8.97 cm	reconfigurable reflectarray antenna for TX necessary, or two different TX antennas
Effective TX antenna height $h_{a,TX}$ for shallow incidence angle	16.6 cm	
TX antenna length $L_{a,TX}$	4.14 m	
Effective RX antenna height $h_{a,RX}$	1.656 m	
Single RX antenna length $L_{a,RX}$	2 m	
Overall RX antenna length	10 m	
TX antenna gain G_{TX} for steep incidence angle	47.25 dBi	antenna efficiency of $\eta_{TX} = 0.8$ assumed
TX antenna gain G_{TX} for shallow incidence angle	49.92 dBi	
Single RX antenna gain G_{RX}	56.75 dBi	antenna efficiency of $\eta_{RX} = 0.8$ assumed; SCORE needed for each RX antenna to achieve the required NESZ

reasonable probability of detection (cf. Fig. 5 top right) and azimuth position accuracy (cf. Fig. 5 bottom left) is achieved.

The line-of-sight velocity estimation accuracy σ_{vr0} and the across-track velocity estimation accuracy σ_{vy0} , which are not plotted, are directly proportional to the azimuth position accuracy σ_x . The corresponding equations for computing these velocity accuracies are:

$$\sigma_{vr0} = \left| -\frac{v_p}{r_{10}} \right| \cdot \sigma_x, \quad \sigma_{vy0} = \frac{\sigma_{vr0}}{\sin \theta_i} \quad (6)$$

where r_{10} is the range to the target. For the given acquisition geometry in Table 2 and an incidence angle of 34° , an azimuth position accuracy of 30 m corresponds to 0.48 m/s (= 1.72 km/h) line-of-sight velocity estimation accuracy and to 0.85 m/s (= 3.07 km/h) across-track velocity estimation accuracy.

The along-track velocity is computed from the estimated Doppler slope of the moving target signal. The results are plotted in Fig. 5 bottom right. The along-track velocity estimation accuracy is in the range from 5 to 20 km/h for the 10 and 3 dBm² target. Note that for all Monte Carlo simulations the absolute along-track velocity of the simulated target was fixed to 0 m/s for avoiding additional (computation time consuming) iterations in the Monte Carlo simulation. The absolute value of the along-track velocity is less important since it has no significant impact on the Doppler slope estimation accuracy and, hence, on the along-track velocity estimation accuracy.

HRWS-GMTI SYSTEM CONCEPT AND PERFORMANCE FOR HRWS-STAP PROCESSING

For HRWS-STAP the M -channel HRWS reference system needs to be extended by a number of N additional RX channels. The HRWS-STAP GMTI performance obtained from Monte Carlo simulations is depicted in Fig. 6 for a different number of RX channels and a fixed target RCS of 3 dBm². All plots are for an incidence angle of $\theta_i = 34^\circ$ and a clutter reflectivity of -6 dB. For a total number of 9 and 11 RX antennas the performance is close to the HRWS-DPCA performance of a 10-channel system (cf. Fig. 5).

For a total number $M + N = 7$ RX antennas the azimuth re-displacement error is better than 60 m outside the blind velocity regions (cf. Fig. 6 bottom left). For 9 RX channels the azimuth re-displacement error even drops to 30 m. The probability of detection and the minimum detectable line-of-sight velocities (cf. Fig. 6 top right) are comparable with

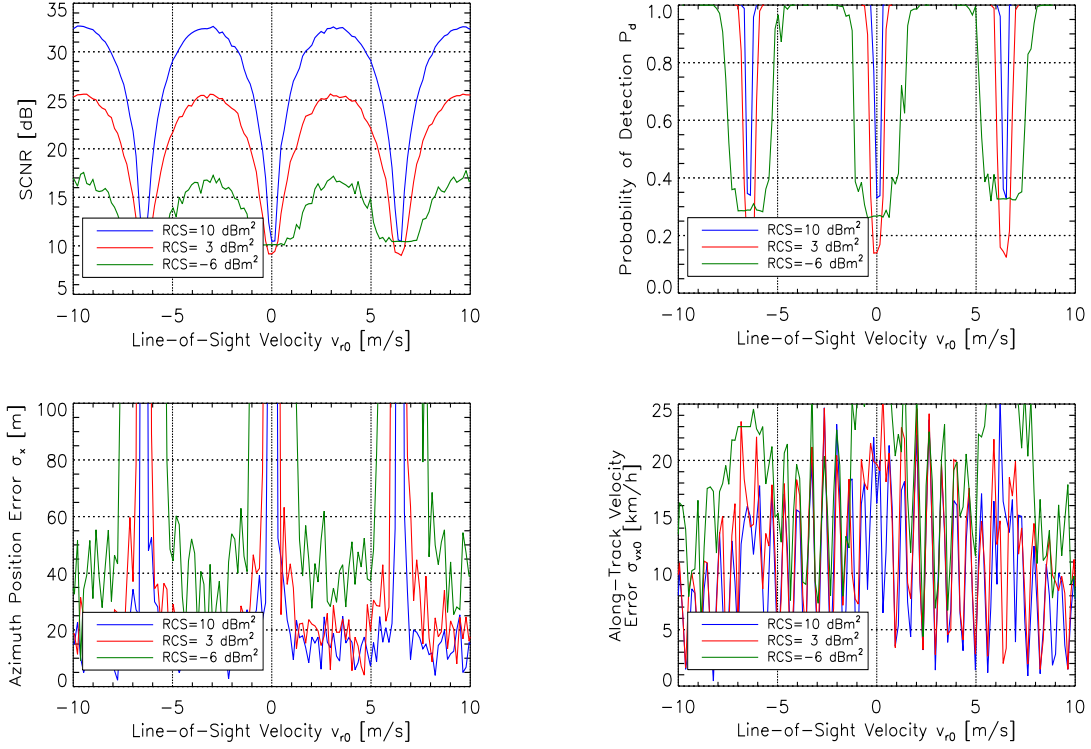


Fig. 5. HRWS-DPCA GMTI performance of a 10-channel HRWS-GMTI system with parameters given in Table 2 (top left: output SCNR; top right: probability of detection for $P_{fa} = 10^{-6}$; bottom left: azimuth position error; bottom right: along-track velocity estimation error; further parameters: $G_{TX} = 47.25$ dBi, 10 RX antennas; incidence angle $\theta_1 = 34^\circ$, $PRF = 1533$ Hz, clutter reflectivity $\sigma_0 = -6$ dB).

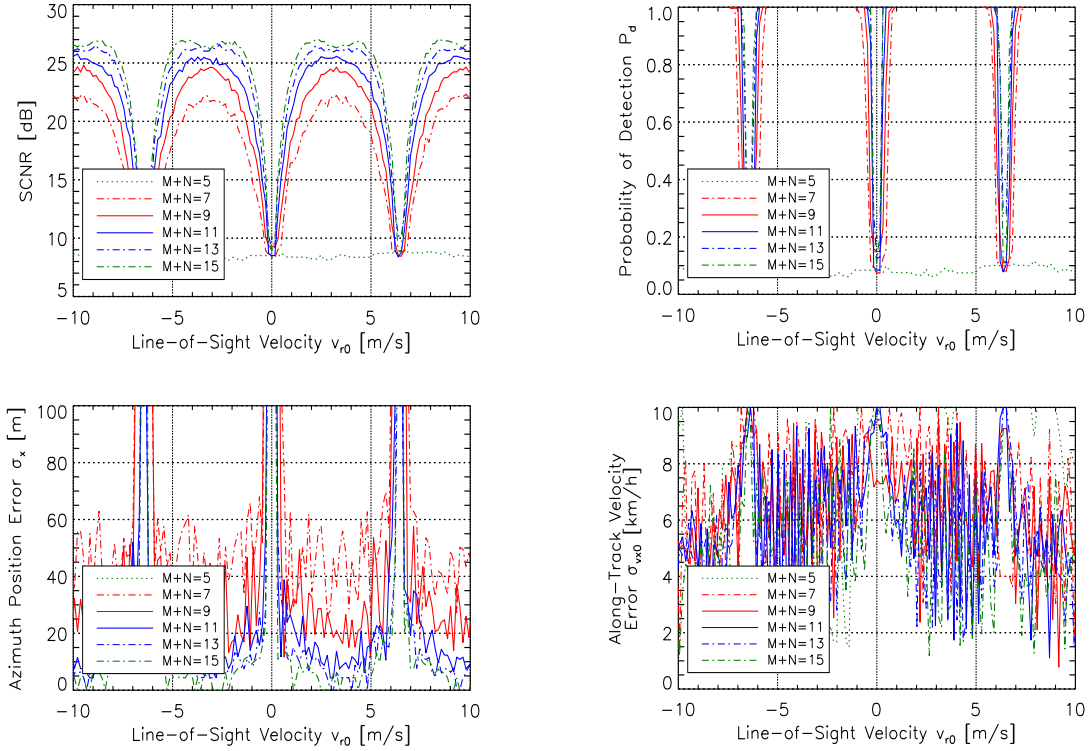


Fig. 6. HRWS-STAP GMTI performance of a HRWS system with a variable number of N additional RX channels with parameters given in Table 2 (top left: output SCNR; top right: probability of detection for $P_{fa} = 10^{-6}$; bottom left: azimuth position error; bottom right: along-track velocity estimation error; further parameters: $G_{TX} = 47.25$ dBi, $5 + N$ RX antennas; incidence angle $\theta_1 = 34^\circ$, $PRF = 1533$ Hz, 3 dBm² target RCS, clutter reflectivity $\sigma_0 = -6$ dB).

the results obtained from the 10-channel HRWS-DPCA system for the 3 dBm² target. The along-track velocity estimation accuracy is better than 10 km/h except for the 5-channel configuration (cf. Fig. 6 bottom right, green dotted line), where nearly no clutter suppression is performed as indicated by the low SCNR value (cf. Fig. 6 top left). Compared with the along-track velocity estimation accuracies obtained with HRWS-DPCA, the HRWS-STAP algorithm provides more accurate along-track velocity estimates over the entire line-of-sight velocity range.

CONCLUSION

Two different HRWS-GMTI algorithms, which we call HRWS-DPCA and HRWS-STAP, were presented. A 5-channel Ka-band reference HRWS system was designed which then was extended by additional RX channels for improving the clutter suppression capability. It was shown by Monte Carlo simulations that with the extended reference system and the proposed algorithms a good HRWS-GMTI performance can be achieved. With the proposed methods and algorithms HRWS SAR imaging and wide-swath GMTI can be performed simultaneously without changing the system operation mode.

REFERENCES

- [1] S. V. Baumgartner, C. Schaefer, and G. Krieger, "Simultaneous Low PRF GMTI and HRWS SAR Imaging without Changing the System Operation Mode," in 10th European Conference on Synthetic Aperture Radar (EUSAR), Berlin, Germany, June 2014.
- [2] ESA/ESTEC "Statement of Work for the Study of Multi-channel Ka-band SARs for moving target indication," TEC-ETP/2011.96/DP, Issue 1.0, 06/07/2011.
- [3] DLR, EADS Astrium and ISEL, "Study of Multi-channel Ka-band SARs for moving target indication – MTI-SAR: MTI Multi-channel Techniques Survey and Scenario Definition," Document No. D1-4000105042, Issue 1.1, 11. June 2012.
- [4] N. Gebert, G. Krieger, and A. Moreira, "Digital Beamforming on Receive: Techniques and Optimization Strategies for High-Resolution Wide-Swath SAR Imaging," *IEEE Transactions on Aerospace and Electronic Systems*, vol. 45, no. 2, pp. 564–592, April 2009.
- [5] C. Schaefer and S. Baumgartner, "Synthetisches Apertur Radar zur gleichzeitigen Bildaufnahme und Bewegtzilerkennung," German Patent 10 2012 021 010.8, pending.
- [6] C. Schaefer and S. Baumgartner, "Ka-Band Instrument for Ground Moving Target Indication with Low PRF Requirement," in Proceedings of 19th Ka and Broadband Communications, Navigation and Earth Observation Conference, vol. 3, Florence, Italy, October 14-17 2013.
- [7] D. Cerutti-Maori, "Adaptive cancellation of azimuth ambiguities for high-resolution wide-swath SAR systems with a multi-channel architecture," Report of ESA Contract No. 4000103561/11/NL/CBi, June 2012.
- [8] D. Cerutti-Maori, I. Sikaneta, J. Klare and C.H. Gierull, "MIMO SAR Processing for Multichannel High-Resolution Wide-Swath Radars," *IEEE Transactions on Geoscience and Remote Sensing*, vol. 52, no. 8, pp. 5034–5055, August 2014.
- [9] D. Cerutti-Maori, I. Sikaneta and C.H. Gierull, "Detection and Imaging of Moving Objects with High-Resolution Wide-Swath SAR Systems," Proceedings the 10th European Conference on Synthetic Aperture Radar (EUSAR), pp. 977-980, Berlin, Germany, 3.-5. July 2014.